

## Article

# Temperature-Dependent and Time-Resolved Luminescence Characterization of $\gamma$ -Ga<sub>2</sub>O<sub>3</sub> Nanoparticles

Marina García-Carrión<sup>1</sup>, Julio Ramírez-Castellanos<sup>2</sup> , Emilio Nogales<sup>1</sup> and Bianchi Méndez<sup>1,\*</sup> <sup>1</sup> Department of Materials Physics, Faculty of Physical Sciences, University Complutense of Madrid, E-28040 Madrid, Spain<sup>2</sup> Department of Inorganic Chemistry, Faculty of Chemical Sciences, University Complutense of Madrid, E-28040 Madrid, Spain

\* Correspondence: bianchi@ucm.es

**Abstract:** The temperature-dependent luminescence properties of  $\gamma$ -Ga<sub>2</sub>O<sub>3</sub> nanoparticles prepared by a precipitation method are investigated under steady-state and pulsed-light excitation. The main photoluminescence (PL) emission at room temperature consists of a single blue band centered around 2.76 eV, which hardly undergoes a blueshift of 0.03 eV when temperature goes down to 4 K. The emission behaves with a positive thermal quenching following an Arrhenius-type curve. The data fitting yields two non-radiative levels affecting the emission band with activation energies of 7 meV and 40 meV. On the other hand, time-resolved PL measurements have also been taken and studied as a function of the temperature. The data analysis has resulted in two lifetimes: one of 3.4 ns and the other of 32 ns at room temperature, which undergo an increase up to 4.5 ns and 65 ns at T = 4 K, respectively. Based on both stationary and dynamic PL results, a model of radiative and non-radiative levels associated with the main emission bands of  $\gamma$ -Ga<sub>2</sub>O<sub>3</sub> is suggested. Finally, by using PL excitation measurements, an estimation of the bandgap and its variation with temperature between 4 K and room temperature were obtained and assessed against O'Donnell–Chen's law. With this variation it has been possible to calculate the average of the phonon energy, resulting in  $\langle \hbar\omega \rangle = 10 \pm 1$  meV.

**Keywords:** gallium oxide; gamma phase; nanoparticle; luminescence; decay time

**Citation:** García-Carrión, M.; Ramírez-Castellanos, J.; Nogales, E.; Méndez, B. Temperature-Dependent and Time-Resolved Luminescence Characterization of  $\gamma$ -Ga<sub>2</sub>O<sub>3</sub> Nanoparticles. *Nanomaterials* **2023**, *13*, 1445. <https://doi.org/10.3390/nano13091445>

Academic Editor: Wan Sik Hwang

Received: 31 March 2023

Revised: 21 April 2023

Accepted: 21 April 2023

Published: 23 April 2023



**Copyright:** © 2023 by the authors. Licensee MDPI, Basel, Switzerland. This article is an open access article distributed under the terms and conditions of the Creative Commons Attribution (CC BY) license (<https://creativecommons.org/licenses/by/4.0/>).

## 1. Introduction

Gallium oxide is a wide-bandgap material with great potential in optoelectronic applications, mainly due to its ultra-wide bandgap (4.7–4.9 eV), chemical stability and polymorphous nature. In particular, five Ga<sub>2</sub>O<sub>3</sub> crystalline phases have been reported, with  $\beta$ -Ga<sub>2</sub>O<sub>3</sub> (monoclinic) being the most-stable and -studied phase. However,  $\alpha$  (orthorhombic),  $\gamma$  (cubic),  $\delta$  (cubic bcc), and  $\epsilon$  (hexagonal) phases, although metastable, are also under investigation since they could provide further tunability of their physical properties or an improvement in the performance of devices that use  $\beta$ -Ga<sub>2</sub>O<sub>3</sub> [1,2]. Among them, the  $\gamma$ -phase is one of the less studied, with little knowledge about its structural and physical properties so far. The crystalline structure has been reported as a distorted cubic spinel structure with a lattice parameter of 8.237 Å [3]. The energy bandgap has been theoretically estimated to be 4.4 eV for the indirect transition and 5.0 eV for the direct transition [4], with no data from experimental measurements yet reported. Some of the applications of the polymorphs of Ga<sub>2</sub>O<sub>3</sub> are linked to photocatalysis or to solar energy conversion. For example, the photocatalytic activity of Ga<sub>2</sub>O<sub>3</sub> nanoparticles (NPs) of several phases ( $\alpha$ ,  $\beta$  and  $\gamma$ ), for the destruction of volatile aromatic pollutants in air or for water splitting, have been recently explored [5,6]. It has been reported that although  $\beta$ -Ga<sub>2</sub>O<sub>3</sub> NPs would exhibit better performance due to their good crystal quality in comparison with other polymorphs,  $\gamma$ -Ga<sub>2</sub>O<sub>3</sub> NPs may play an excellent role in photocatalytic applications because of their high oxygen-vacancy concentration as a consequence of the not-so-perfect crystallization of this

phase [7]. Regarding solar energy conversion, the use of nanocomposites with  $\gamma$ -Ga<sub>2</sub>O<sub>3</sub> NPs has been proven to be a better passivation material compared to those that embedded  $\beta$ -Ga<sub>2</sub>O<sub>3</sub> NPs [8]. In this later case, the reason for this performance enhancement is still not well understood. In the aforementioned applications, there is a better knowledge of the light absorption and emission properties of  $\gamma$ -Ga<sub>2</sub>O<sub>3</sub> and a better understanding of the potential improvement of their usage in devices. To that end, the investigation of optical properties related to the presence of native defects, such as the oxygen vacancies, in  $\gamma$ -Ga<sub>2</sub>O<sub>3</sub> NPs is required. The literature about the optical properties of this phase is scarce. A few works have reported the photoluminescence (PL) of colloidal Ga<sub>2</sub>O<sub>3</sub> nanocrystals of different sizes [9,10]. However, studies of time-resolved and temperature-dependent PL measurements have not been reported yet.

One of the challenges in the research of polymorphic materials is the selection of a suitable synthesis route. In particular, the synthesis of Ga<sub>2</sub>O<sub>3</sub>-based nanomaterials has been tackled under many approaches, including physical and chemical methods, to produce the desired nanomaterial [11]. In the case of Ga<sub>2</sub>O<sub>3</sub> nanoparticles, the hydrothermal method [12], the solution combustion route [13] or the controlled precipitation route [5] are rather simple and cost-effective techniques. Among them, the precipitation route allows for a fine tuning of the microstructure by accurately controlling the pH of the solution. The method offers a valid and reliable way to synthesize several polymorphs via the simple control of the synthesis conditions, such as temperature, reaction time, pH or atmosphere. Herein, we have used the precipitation method to achieve chemically stable  $\gamma$ -Ga<sub>2</sub>O<sub>3</sub> NPs. In some applications, such as in photocatalysis, as-grown material can be used directly; however, applications in optoelectronic or power electronic devices would require further processing steps to achieve suitable assemblies, as heterostructures, which become active elements in the devices.

In this work, the temperature-dependent luminescence properties of  $\gamma$ -Ga<sub>2</sub>O<sub>3</sub> nanoparticles prepared by a precipitation method are investigated under steady-state and pulsed-light excitation. The analysis of the PL results obtained under stationary and dynamic conditions has allowed us to suggest some radiative and non-radiative levels associated with the main emission bands of  $\gamma$ -Ga<sub>2</sub>O<sub>3</sub>. In addition, by using photoluminescence excitation (PLE) measurements, an estimation of the bandgap and its variation with temperature between 4 K and room temperature was obtained for the first time and assessed against the empirical Varshni and O'Donnell formulae.

## 2. Materials and Methods

In this experiment,  $\gamma$ -Ga<sub>2</sub>O<sub>3</sub> NPs were prepared by a precipitate method by dissolving gallium nitrate hydrate (Ga(NO<sub>3</sub>)<sub>3</sub> × H<sub>2</sub>O) in distilled water, as explained elsewhere [1]. Ammonium hydroxide solution was slowly added into that solution to obtain a basic pH (pH~8). The resultant precipitate was filtered and dried in air. The obtained powder was calcined in air at 250 °C for 14 h.

The structural characterization was carried out by means of X-ray diffraction, performed with a PANalytical X'Pert MPD (CuK<sub>α</sub> irradiation,  $k = 1.5404 \text{ \AA}$ ) system. In addition, Raman spectroscopy was conducted with a Horiba Jobin Yvon LabRAM HR800 confocal microscope. Luminescence properties were assessed by photoluminescence (PL), and PLE and time-resolved PL (TR-PL) techniques were performed in an Edinburgh Instruments FLS1000 spectrometer equipped with a continuous 450 W Xe lamp and a pulsed LED with  $\lambda_{\text{exc}} = 256.8 \text{ nm}$ . The system was also equipped with an Oxford Instruments cryostat that allows measurements in the 4–300 K temperature range. Transmission electron microscopy (TEM) and high-resolution TEM (HRTEM) measurements were performed in a JEOL 300 at the ICTS-CNM facility.

## 3. Results

Figure 1a shows the XRD pattern of the  $\gamma$ -Ga<sub>2</sub>O<sub>3</sub> nanoparticles (NPs). The maxima can be assigned to the cubic structure, space group Fd3/m, with the lattice parameter

$a = 8.24 \text{ \AA}$  (ICDD: 01-082-3194) of the  $\gamma\text{-Ga}_2\text{O}_3$ , in agreement with other works [4]. No peaks associated to other  $\text{Ga}_2\text{O}_3$  phases are found. The broad peaks are a hint of the small size of the particles and of a not-perfect crystallization. The two peaks marked with an asterisk in the plot are associated with the material of the sample holder used for these measurements. The XRD diffractogram agrees with those reported by other authors [5] in  $\gamma\text{-Ga}_2\text{O}_3$  NPs obtained by similar routes. The average crystal size was calculated from the values of the form factor  $K$ , the wavelength of the incident radiation  $\lambda$ , the full width at half maximum  $B$  of the diffraction maximum (311), and the diffraction angle  $\theta$ , all of them provided by the ICDD, along with the Scherrer formula:  $D = K \cdot \lambda / (B \cos \theta)$ . The mean value is  $9.43 \pm 0.02 \text{ nm}$ . This value is slightly higher than the crystal sizes reported in the literature of  $\gamma\text{-Ga}_2\text{O}_3$  NPs synthesized by precipitation or combustion-based methods, which are about 3–5 nm [5,13].

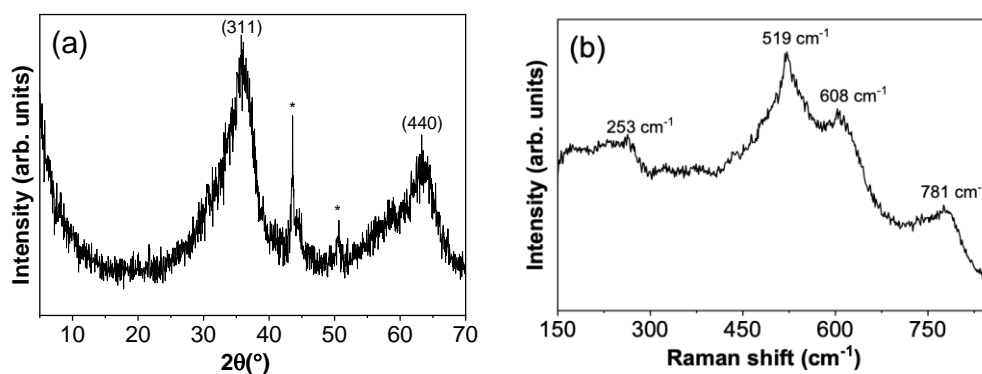


**Figure 1.** (a) XRD diffractogram from nanocrystalline  $\gamma\text{-Ga}_2\text{O}_3$ . Peaks labeled with an asterisks correspond to the sample holder. (b) Raman spectrum from  $\gamma\text{-Ga}_2\text{O}_3$  nanocrystals using a He-Cd laser with 325 nm.

To further investigate the crystalline ordering, Raman spectroscopy measurements were carried out and the results are shown in Figure 1b. The Raman spectrum presents some broad peaks, as expected from the XRD diffraction characterization. In spite of that, some peaks can be resolved for the vibration modes of this phase centered at 253, 519, 608, 781  $\text{cm}^{-1}$ , possibly attributed to the tension and bending movement of the Ga-O bonds. To our knowledge, there are few Raman studies on  $\gamma\text{-Ga}_2\text{O}_3$  NPs, and they also report broad peaks that would be related to the small average size of the nanoparticles and a weak Raman response [5,13]. Hence, it is not possible to correlate the Raman modes with specific symmetries.

Low-magnification TEM and HRTEM images of  $\gamma\text{-Ga}_2\text{O}_3$  NPs are shown in Figure 2. A nanoparticle conglomerate is shown in Figure 2a, where crystallites of sizes clearly below 20 nm are observed, in agreement with the value calculated by Scherrer's formula from X-ray diffraction. Figure 2b shows a high-resolution TEM image in which an interplanar distance of 2.46  $\text{\AA}$  was measured. This value corresponds to the XRD peak assigned to the (311) plane in Figure 1. Finally, it is worth mentioning that the TEM images suggest that part of the material is amorphous, which is consistent with the broad peaks observed both in XRD (Figure 1a) and Raman spectroscopy (Figure 1b) results.

We now proceed with the study of the luminescence properties of the  $\gamma\text{-Ga}_2\text{O}_3$  NPs. Figure 3 shows the PL and PLE spectra obtained at room temperature (RT). The PL emission spectrum was acquired with an excitation energy of 4.7 eV while the PLE excitation spectrum was obtained collecting emitted photons with a 2.7 eV emission. It is observed that the PL emission is dominated by a broad visible band, with the maximum around 2.66 eV (466 nm). This blue emission can be attributed to donor-acceptor transitions (DAP) involving deep donors and acceptors, due to the presence of intrinsic point defects such as oxygen vacancies ( $V_{\text{O}}$ ) acting as donors and Ga vacancies or Ga-O vacancies pairs ( $V_{\text{Ga}}$ ,  $V_{\text{Ga}} - V_{\text{O}}$ ) acting as acceptor centers, which agrees with published results [14–16]. The

rather high intensity of this visible emission would imply a high density of point defects in the nanoparticles, which is consistent with the above structural results. On the other hand, the PLE spectrum yields a band with a maximum at 4.72 eV that could be linked to the energy bandgap of the  $\gamma$ -Ga<sub>2</sub>O<sub>3</sub>. This broad visible emission could be of interest in the design of white light-emitter devices as an alternative to the selective rare-earth doping of Ga<sub>2</sub>O<sub>3</sub> to simultaneously achieve red, green and blue emission lines [17].

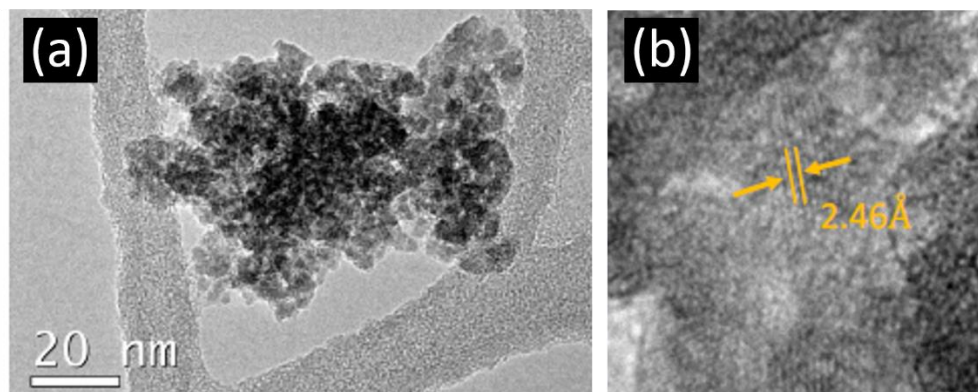


**Figure 2.** (a) Low-magnification TEM image of the  $\gamma$ -Ga<sub>2</sub>O<sub>3</sub> nanocrystals, (b) HRTEM image of one nanoparticle from the agglomerate shown in (a).

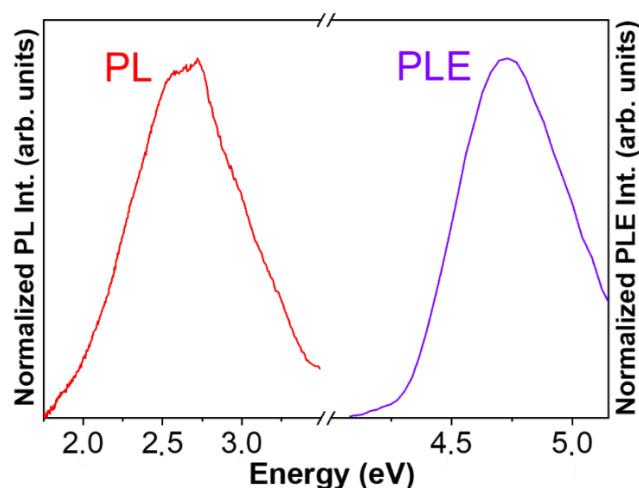


**Figure 3.** PL (red line) and PLE (purple line) spectra of  $\gamma$ -Ga<sub>2</sub>O<sub>3</sub> nanoparticles acquired at RT. PL was excited with photons of 4.7 eV. PLE was acquired monitoring the emitted photons of 2.7 eV energy.

To better understand the recombination mechanisms and the kinetics of the luminescence related to point defects in these nanoparticles, both steady-state and pulsed excitation probes have been used along with the study of both PL and PLE spectra in a range of temperatures from  $T = 4$  K to RT. In doing so, information about the activation energies of defect-related energy levels involved in the emission and radiative and non-radiative lifetimes can be determined. In addition, the monitoring of the PLE band with temperature allows us to investigate the temperature dependence of the bandgap of  $\gamma$ -Ga<sub>2</sub>O<sub>3</sub> [18–20].

The PL spectra series, excited with a photon energy of 4.9 eV, is displayed in Figure 4a. Figure 4b shows the corresponding contour map of the integrated PL emission as a function of the temperature. It is observed that the PL intensity increases as the temperature decreases, which means a luminescence thermal quenching. Single spectra at RT and at  $T = 4$  K are shown in Figure 4c,d, respectively, along with their deconvolutions into Gaussian functions. In both cases, a nice deconvolution was obtained with a single band, centered at 2.79 eV at 4 K and at 2.76 eV at RT, which we will call the  $\gamma$ -vis band. It is worth

noticing that there is almost no shift of this broad emission band as the temperature varies. On the other hand, the features appearing on the high-energy side of the emission band are regarded as artifacts, after trials under different conditions.

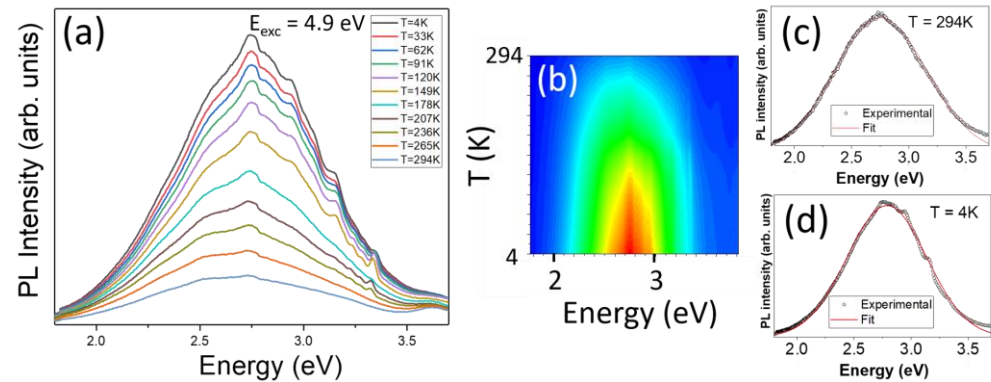


**Figure 4.** (a) PL spectra as a function of temperature with an excitation energy 4.9 eV. (b) Contour map of the integrated PL versus temperature. Deconvolution of the PL spectra at (c) RT and (d)  $T = 4$  K.

The PL thermal quenching of luminescence bands related to defect points is often assessed against the following empirical formula that takes into account an eventual number of non-radiative energy levels,  $i$ , that compete with the main radiative level [21,22]:

$$I_{\text{PL}}(T) = \frac{I_0}{1 + \sum_i A_i \exp(-E_i/k_B T)} \quad (1)$$

where  $I_0$  would be the PL intensity at very low temperature,  $A_i$  are constants, and  $E_i$  are the activation energies of non-radiative levels. The physical meaning of the  $A_i$  constants is not quite clear and depends on the model used to understand the PL thermal quenching in each case [22]. However, in oxides with emission bands related to native defects, the coefficients  $A_i$  could be related to the ratio between the luminescence radiative lifetime  $\tau_R$  and the non-radiative lifetime  $\tau_{NR}$  [21].

Figure 5 shows the evolution of the PL intensity with respect to the temperature obtained from each deconvolution of the PL spectra shown in Figure 4a along with the fitting of experimental data to Equation (1). In this case, it has been necessary to consider two non-radiative levels with activation energies  $E_1$  and  $E_2$ , since otherwise the thermal excitation process saturates at low temperatures. Assuming a main radiative level,  $E_R$ , as that responsible for the observed PL band,  $E_i$  stands for the difference between each non-radiative level and the radiative level, being  $E_1 = E_{NR1} - E_R$  and  $E_2 = E_{NR2} - E_R$ . The fitting results of the PL experimental data yields the values of  $A_1 = 0.7 \pm 0.2$  and  $E_1 = 7 \pm 1$  meV and  $A_2 = 14 \pm 3$  and  $E_2 = 40 \pm 4$  meV, which are summarized in Table 1. The line profile of PL variation allows us to distinguish two regions: one at low temperatures ( $<60$  K) with an almost constant PL intensity and another one at higher temperatures ( $>60$  K) with a sharp decrease in PL intensity. This “threshold” temperature agrees with the presence of the closest energy level ( $E_1$ ) that saturates at around 60 K. Even though the higher energy level  $E_{NR2}$  would require a very high temperature to be activated, both non-radiative levels could be related to surface states when taking into account the surface-to-bulk ratio in the case of nanoparticles. These states would act as traps for carriers favoring the luminescence quenching in the  $\gamma$ -vis emission.

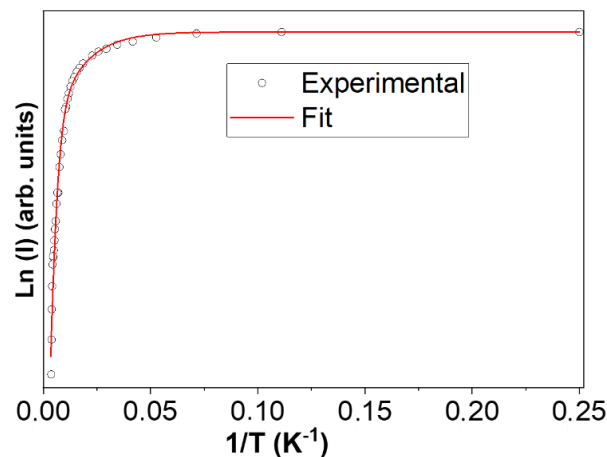


**Figure 5.** PL intensity of the  $\gamma$ -vis band represented as a function of  $1/T$ . Dots are experimental data from recorded PL spectra at each temperature and red line is the result of the data fitting to Equation (1).

**Table 1.** Fitting parameters of the PL thermal quenching to Equation (1).

Energy Level	Activation Energy $E_i$ (meV)	Constant
$E_1$	$7 \pm 1$	$0.7 \pm 0.2$
$E_2$	$40 \pm 4$	$14 \pm 3$

In order to obtain more information about the luminescence kinetics in the  $\gamma$ -Ga<sub>2</sub>O<sub>3</sub> NPs, time-resolved (TR)-PL measurements were taken by exciting with a pulsed LED ( $\lambda_{exc} = 256$  nm) over a range of temperatures between 4 K and RT, which allowed us to study the PL lifetime temperature dependence. Figure 6a shows the PL intensity decay at room temperature (pink line) and 4 K (black line), which show an exponential time decay. Two exponential functions, with characteristic lifetimes  $t_1$  and  $t_2$ , are needed to obtain an accurate matching with the experimental data, according to the following equation [23,24]:

$$I_{PL}(t) = A \exp(-t/\tau_1) + B \exp(-t/\tau_2) \quad (2)$$

Generally, the effective lifetime can be expressed as  $1/\tau = 1/\tau_R + 1/\tau_{NR}$  when taking into account both radiative and non-radiative recombination. However, when considering the thermal population of the energy levels of the emission-related center, the lifetime dependence with the temperature can be expressed as follows:

$$\frac{1}{\tau} = \frac{1}{\tau_R} + \frac{e^{-\Delta E/k_B T}}{\tau_{NR}} \quad (3)$$

where  $\Delta E$  is the separation energy between the radiative and non-radiative levels,  $\tau_R$  is the radiative recombination time and  $\tau_{NR}$  are the lifetime of non-radiative decays. By fitting the PL decay curves of Figure 6a to Equation (2), the two lifetimes obtained for the g-vis emission band at each temperature are:  $\tau_1$  (RT) =  $(3.4 \pm 0.1)$  ns and  $\tau_2$  (RT) =  $(32 \pm 4)$  ns, while  $\tau_1$  (4 K) =  $(4.5 \pm 0.1)$  ns and  $\tau_2$  (4 K) =  $(67 \pm 2)$  ns. This variation of lifetime with temperature could be related to the different electron occupation of the energy levels in thermally activated processes, since the lifetime is inversely proportional to the free electrons. In our case, it can be noticed that there is a slight decrease in one process ( $\Delta\tau_1 = 1.1$  ns) and an increase in the second characteristic calculated lifetime ( $\Delta\tau_2 = 35$  ns) in the explored temperature range.

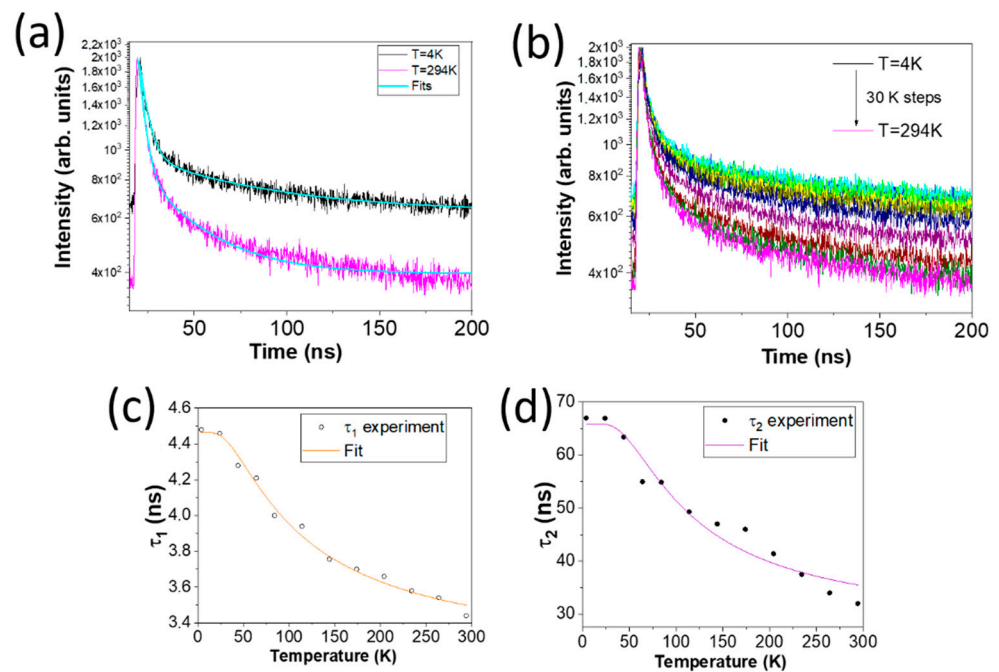


**Figure 6.** (a) PL intensity as a function of time at 4 K (black line), at RT (pink line) and fitting curves (blue lines) to Equation (2). (b) PL intensity series as a function of time used to determine the lifetime decays at 30 K temperature intervals. (c)  $\tau_1$  (T) and (d)  $\tau_2$  (T) calculated lifetimes (white and black dots) along with the fitting curves to Equation (3).

In order to better understand the temperature dependence, a series of TR-PL spectra have been recorded over a range of temperatures between 4K and RT, as represented in Figure 6b. From each curve, the values of  $\tau_1(T)$  and  $\tau_2(T)$  can be obtained and fitted to Equation (3). Figure 6c,d show the calculated lifetimes (white and black dots) of  $\tau_1$  and  $\tau_2$ , respectively, along with the resulting curves from the fitting of these data to Equation (3). Table 2 summarizes the results obtained for  $\Delta E$ ,  $\tau_R$  and  $\tau_{NR}$  for the two lifetimes.

**Table 2.** Data obtained from the temperature-dependence lifetime study.

$\tau_1$			$\tau_2$		
$\tau_{R1}$ (ns)	$\tau_{NR1}$ (ns)	$\Delta E_1$ (meV)	$\tau_{R2}$ (ns)	$\tau_{NR2}$ (ns)	$\Delta E_2$ (meV)
$11 \pm 1$	$4.5 \pm 0.1$	$10 \pm 1$	$66 \pm 2$	$44 \pm 9$	$15 \pm 2$

Based on what has been explained above from our results, the recombination center deduced from  $\tau_1(T)$ ,  $\Delta E_1$ , could be assigned to that one,  $E_1$ , deduced from the  $I_{PL}(T)$  curves. On the other hand, the second level observed by TR-PL ( $\Delta E_2$ ) could also influence the evolution of  $I_{PL}(T)$ .

Finally, we study the evolution of the bandgap with the temperature for the  $\gamma$ -Ga<sub>2</sub>O<sub>3</sub> NPs by means of the analysis of the PLE spectra measured at different temperatures, as presented in Figure 7a. At RT, the main observed band is centered around 4.7 eV and shifts to almost 5 eV when the temperature is lowered to 4 K. The PLE series spectra have been deconvoluted, as Figure 7b,c show for the RT and 4K cases, respectively. In doing so, three bands can be resolved. Band 1 (blue line) is possibly related to shallow donors and band 2 may represent the bandgap of the  $\gamma$ -Ga<sub>2</sub>O<sub>3</sub>, with a redshift from 4.93 eV at 4 K to 4.74 eV at RT. These values agreed with the only reported calculated value for the energy bandgap in  $\gamma$ -Ga<sub>2</sub>O<sub>3</sub>.

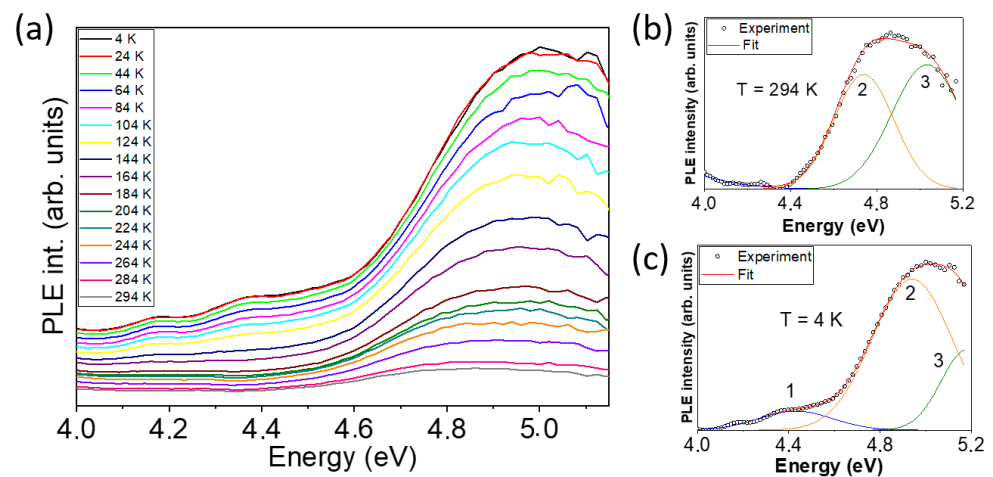


**Figure 7.** (a) PLE spectra as a function of temperature for an emission energy of 2.75 eV. Deconvolution of the PLE spectra (b) at room temperature and (c) at 4 K.

Several empirical formulae have been proposed to study the bandgap temperature dependence, which usually decreases as temperature increases. This is associated to the dilatation of the crystalline lattice that alters the relative positions of the valence and conduction bands. Since the thermal expansion at low temperatures is not linear, Varshni proposed a formula (Equation (4)) in which the parameter  $\alpha$  represents the slope limit at very high temperatures, and the parameter  $\beta$  is related to the Debye temperature. However, the Varshni law does not fit the bandgap temperature dependence in some materials, such as diamond or SiC, which have small thermal-expansion coefficients and the electron-phonon interaction would be the main factor affecting the bandgap shift with the temperature. O'Donnell and Chen proposed an alternative expression (Equation (5)) that usually renders a better fit to experimental results, in which  $S$  is a nondimensional constant related to the strength of the electron-phonon interaction and  $\langle \hbar\omega \rangle$  is an average of phonon energy [25]:

$$E_g(T) = E_g(0) - \frac{\alpha T^2}{\beta + T} \quad (4)$$

$$E_g(T) = E_g(0) - S \langle \hbar\omega \rangle \left[ \coth\left(\frac{\langle \hbar\omega \rangle}{2k_B T}\right) - 1 \right] \quad (5)$$

Figure 8 shows the bandgap values calculated from the fitting of the PLE spectra at different temperatures (open dots) as well as the fitting curve of these data to the O'Donnell and Chen equation (continuous line) and to the Varshni equation (dashed line). The parameters resulting in the Varshni model are  $\alpha = 0.19$  meV/K and  $\beta = 558 \pm 20$  K. The  $\beta$  parameter has been reported for the case of the nanoparticles of  $\gamma$ -Ga<sub>2</sub>O<sub>3</sub>, giving an approximate value of 580 K [10], which is similar to that obtained here. On the other hand, the values of  $\langle \hbar\omega \rangle = 10 \pm 1$  meV,  $S = (4.59 \pm 0.12) \times 10^{-4}$  and  $E_g(0) = 4.74$  eV are obtained from the equation proposed by O'Donnell and Chen. No previous works have been found on the  $S$  parameter nor on the average phonon energy in  $\gamma$ -Ga<sub>2</sub>O<sub>3</sub>. Herein, it can be observed that the O'Donnell and Chen model matches rather better than the Varshni model with our calculated results. This is consistent with the low thermal-expansion coefficients of Ga<sub>2</sub>O<sub>3</sub> that were reported for the  $\beta$ -phase so far [26].

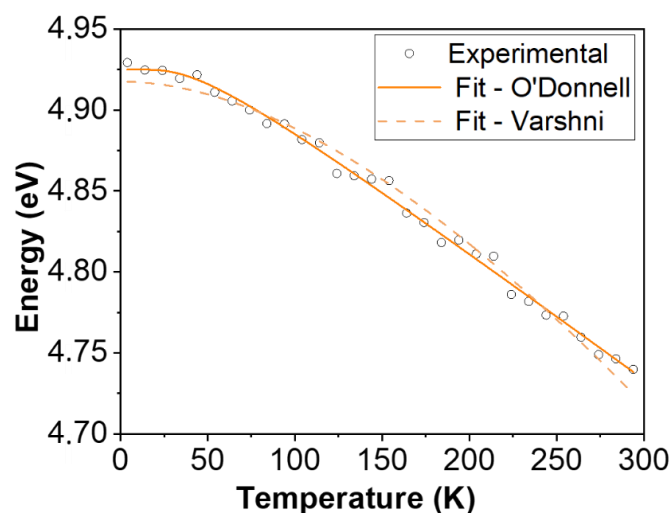


**Figure 8.** Variation in the estimated bandgap with temperature from PLE results. Open dots are calculated data—the continuous line is the fitting to the O'Donnell formula, whereas the dashed line is the fit to the Varshni equation.

#### 4. Conclusions

In the present work, the luminescence properties of  $\gamma$ -Ga<sub>2</sub>O<sub>3</sub> nanocrystals obtained by a precipitation method are presented and discussed. It should be mentioned that hardly any studies have been found on the luminescent properties of this metastable phase of gallium oxide. Through XRD and Raman measurements, it has been verified that the nanoparticles obtained at a temperature of 250 °C exhibit the  $\gamma$ -Ga<sub>2</sub>O<sub>3</sub> phase, as well as the fact that there is no presence of another phase, although some amorphous material remains in the product. In spite of that, the Raman spectra show some vibration modes of the crystallized phase. The PL study has included measurements under steady conditions as well as under a pulsed excitation source. Furthermore, both of them have been carried out over a temperature range from 4 K to RT. The main PL emission is a single band centered around 2.76 eV at room temperature, which hardly shifts when temperature decreases. The origin of this emission could be DAP transitions that involved native defects of  $\gamma$ -Ga<sub>2</sub>O<sub>3</sub>, as is usual in wide-bandgap oxides. The PL intensity as a function of the temperature has been fitted to an Arrhenius-type law, leading to the appearance of two temperature behavior regimes, as a consequence of the non-radiative levels affecting the emission band. These two levels have an activation energy of 7 meV and 40 meV. On the other hand, TR-PL measurements as a function of the temperature have allowed us to determine the lifetimes that control the quantum efficiency and their temperature dependence. The fitting to exponential decays of the PL intensity with time has resulted in two lifetimes: one of 3.4 ns and the other of 32 ns at RT. From the analysis of the shortest one with the temperature, a model of radiative and non-radiative levels associated with the main emission bands of  $\gamma$ -Ga<sub>2</sub>O<sub>3</sub> is proposed, which agrees with the results raised from the Arrhenius fitting of the PL intensity with the temperature. Finally, the bandgap and its variation with temperature between 4 K and room temperature were obtained using PLE spectra, giving rise to a difference of 0.2 eV. The results show a rather good match to the O'Donnell formula, and a value for the average of the phonon energy, resulting in  $\langle \hbar\omega \rangle = 10 \pm 1$  meV, has been deduced.

**Author Contributions:** Conceptualization, B.M. and E.N.; methodology, M.G.-C. and J.R.-C.; validation, M.G.-C., B.M. and E.N.; formal analysis, M.G.-C.; investigation, M.G.-C., B.M. and E.N.; resources, J.R.-C. and B.M.; data curation, M.G.-C.; writing—original draft preparation, E.N. and B.M.; writing—review and editing, all authors; funding acquisition, B.M. All authors have read and agreed to the published version of the manuscript.

**Funding:** This work was supported by MICIN projects (RTI2018-097195-B-I00, M-ERA.NET PCIN-2017-106 and PID2021-122562NB-I00). The authors acknowledge the support from the Air Force Office of Scientific Research under Award No. FA8655-20-1-7013 (Program Manager: Ali Sayir).

**Data Availability Statement:** The data that support the findings of this study are available from the corresponding author upon reasonable request.

**Conflicts of Interest:** The authors declare no conflict of interest.

## References

1. Pearton, S.J.; Yang, J.; Cary IV, P.H.; Ren, F.; Kim, J.; Tadjer, M.J.; Mastro, M.A. A review of Ga<sub>2</sub>O<sub>3</sub> materials, processing, and devices. *Appl. Phys. Rev.* **2018**, *5*, 011301. [[CrossRef](#)]
2. Spencer, J.A.; Mock, A.L.; Jacobs, A.G.; Schubert, M.; Zhang, Y.; Tadjer, M.A. A review of band structure and materials properties of transparent conducting and semiconducting oxides: Ga<sub>2</sub>O<sub>3</sub>, Al<sub>2</sub>O<sub>3</sub>, In<sub>2</sub>O<sub>3</sub>, ZnO, SnO<sub>2</sub>, CdO, NiO, CuO and Sc<sub>2</sub>O<sub>3</sub>. *Appl. Phys. Rev.* **2022**, *9*, 011315. [[CrossRef](#)]
3. Playford, H.Y.; Hannon, A.C.; Barney, E.R.; Walton, R.I. Structures of uncharacterized polymorphs of gallium oxide from total neutron diffraction. *Chemistry* **2013**, *19*, 2803–2813. [[CrossRef](#)] [[PubMed](#)]
4. Oshima, T.; Nakazono, T.; Mukai, A.; Ohtomo, A. Epitaxial growth of g-Ga<sub>2</sub>O<sub>3</sub> films by MIST chemical vapor deposition. *J. Cryst. Growth.* **2012**, *359*, 60–63. [[CrossRef](#)]
5. Hou, Y.; Wu, L.; Wang, X.; Ding, Z.; Li, Z.; Fu, X. Photocatalytic performance of α-, β-, and γ-Ga<sub>2</sub>O<sub>3</sub> for the destruction of volatile aromatic pollutants in air. *J. Catal.* **2007**, *250*, 12–18. [[CrossRef](#)]
6. Li, L.; Ma, B.; Xie, H.; Yue, M.; Cong, R.; Gao, W.; Yang, T. Photocatalytic H<sub>2</sub> evolution for α-, β-, γ-Ga<sub>2</sub>O<sub>3</sub> and suppression of hydrolysis of γ-Ga<sub>2</sub>O<sub>3</sub> by adjusting pH, adding a sacrificial agent or loading a cocatalyst. *RSC Adv.* **2016**, *6*, 59450–59456. [[CrossRef](#)]
7. Zhang, X.; Zhang, Z.; Huang, H.; Wang, Y.; Tong, N.; Lin, J.; Liu, D.; Wang, X. Oxygen vacancy modulation of two-dimensional γ-Ga<sub>2</sub>O<sub>3</sub> nanosheets as efficient catalysts for photocatalytic hydrogen evolution. *Nanoscale* **2018**, *10*, 21509–21517. [[CrossRef](#)]
8. García-Carrión, M.; Ramírez-Castellanos, J.; Nogales, E.; Méndez, B.; You, C.C.; Karazhanov, S.; Marstein, E.S. Hybrid solar cells with β- and γ-gallium oxide nanoparticles. *Mater. Lett.* **2020**, *261*, 127088. [[CrossRef](#)]
9. Wang, T.; Farvid, S.S.; Abulikemu, M.; Radovanovic, P.V. Size tunable phosphorescence in colloidal metastable γ-Ga<sub>2</sub>O<sub>3</sub> nanocrystals. *J. Am. Chem. Soc.* **2010**, *132*, 9250–9252. [[CrossRef](#)]
10. Wang, T.; Radovanovic, P.V. Size-Dependent Electron Transfer and Trapping in Strongly Luminescent Colloidal Gallium Oxide Nanocrystals. *J. Phys. Chem. C* **2011**, *115*, 18473–18478. [[CrossRef](#)]
11. Feng, S.; Qiao, H. Preparations, properties and applications of gallium oxide nanomaterials—A review. *Nano Select* **2022**, *3*, 348–373.
12. Yan, S.; Wan, L.; Li, Z.; Zhou, Y.; Zou, Z. Synthesis of a mesoporous single crystal Ga<sub>2</sub>O<sub>3</sub> nanoplate with improved photoluminescence and high sensitivity in detecting CO. *Chem. Commun.* **2010**, *46*, 6388–6390. [[CrossRef](#)]
13. Seshadri, H.; Cheralathan, M.; Sinha, P.K. Photocatalytic performance of combustion-synthesized β and γ-Ga<sub>2</sub>O<sub>3</sub> in the degradation of 1,4-dioxane in aqueous solution. *Res. Chem. Intermed.* **2013**, *39*, 991–1001. [[CrossRef](#)]
14. Farvid, S.S.; Wang, T.; Radovanovic, P.V. Colloidal gallium indium oxide nanocrystals: A multifunctional light-emitting phosphor broadly tunable by Alloy composition. *J. Am. Chem. Soc.* **2011**, *133*, 6711–6719. [[CrossRef](#)]
15. Shimamura, K.; Villora, E.G.; Ujiie, T.; Aoki, K. Excitation and photoluminescence of pure and Si-doped β-Ga<sub>2</sub>O<sub>3</sub> single crystals. *Appl. Phys. Lett.* **2008**, *92*, 27–30. [[CrossRef](#)]
16. Fernandes, B.; Hegde, M.; Stanish, P.C.; Miškovic, Z.L.; Radovanovic, P.V. Photoluminescence decay dynamics in g-Ga<sub>2</sub>O<sub>3</sub> nanocrystals: The role of exclusion distance at short time scales. *Chem. Phys. Lett.* **2017**, *684*, 135–140. [[CrossRef](#)]
17. Huang, Y.; Saito, K.; Tanaka, T.; Guo, Q. Strategy toward white LEDs based on vertically integrated rare earth doped Ga<sub>2</sub>O<sub>3</sub> films. *Appl. Phys. Lett.* **2021**, *119*, 06210. [[CrossRef](#)]
18. Pankove, J.I. *Optical Processes in Semiconductors*; Courier Corporation: Washington, DC, USA, 1975.
19. Grundmann, M. *Physics of Semiconductors*; Springer: Berlin/Heidelberg, Germany, 2010.
20. Tokida, Y.; Adachi, S. Photoluminescence spectroscopy and energy level analysis of metal-organic-deposited Ga<sub>2</sub>O<sub>3</sub>:Cr<sup>3+</sup> films. *J. Appl. Phys.* **2012**, *112*, 063522. [[CrossRef](#)]
21. Gallart, M.; Cottineau, T.; Hönerlage, B.; Keller, V.; Keller, N.; Pierre Gilliot, P. Temperature dependent photoluminescence of anatase and rutile TiO<sub>2</sub> single crystals: Polaron and self-trapped exciton formation. *J. Appl. Phys.* **2018**, *124*, 133104. [[CrossRef](#)]
22. Reshchikov, M.A. Mechanisms of thermal quenching of defect-related luminescence in semiconductors. *Phys. Status Solidi A* **2021**, *218*, 2000101. [[CrossRef](#)]
23. Nogales, E.; García, J.A.; Méndez, B.; Piqueras, J. Red luminescence of Cr in β-Ga<sub>2</sub>O<sub>3</sub> nanowires. *J. Appl. Phys.* **2007**, *101*, 033517. [[CrossRef](#)]
24. Dovrat, M.; Goshen, Y.; Jedrzejewski, J.; Balberg, I.; Sa'ar, A. Radiative versus nonradiative decay processes in silicon nanocrystals probed by time-resolved photoluminescence spectroscopy. *Phys. Rev. B* **2004**, *69*, 155311. [[CrossRef](#)]

25. O'Donnell, K.; Chen, X. Temperature dependence of semiconductor band gaps. *Appl. Phys. Lett.* **1991**, *58*, 2924–2926. [[CrossRef](#)]
26. Villora, E.G.; Shimamura, K.; Ujiie, T.; Aoki, K. Electrical conductivity and lattice expansion of b-Ga<sub>2</sub>O<sub>3</sub> below room temperature. *Appl. Phys. Lett.* **2008**, *92*, 202118. [[CrossRef](#)]

**Disclaimer/Publisher's Note:** The statements, opinions and data contained in all publications are solely those of the individual author(s) and contributor(s) and not of MDPI and/or the editor(s). MDPI and/or the editor(s) disclaim responsibility for any injury to people or property resulting from any ideas, methods, instructions or products referred to in the content.